Author Manuscript

Author Manuscript

Author Manuscript

Author Manuscript

HHS Public Access

Author manuscript

J Magn Reson Imaging. Author manuscript; available in PMC 2020 June 29.

Published in final edited form as:

J Magn Reson Imaging. 2020 June ; 51(6): 1789–1798. doi:10.1002/jmri.26998.

Scan-rescan repeatability and impact of B_0 and B_1 field non-uniformity corrections in single-point whole-brain macromolecular proton fraction mapping

Vasily L. Yarnykh, PhD[1,2], **Alena A. Kisel, MS**[2], **Marina Y. Khodanovich, PhD**[2]

[1]University of Washington, Department of Radiology, Seattle, WA, United States.

[2]Research Institute of Biology and Biophysics, Tomsk State University, Tomsk, Russian Federation.

Abstract

Background: Single-point macromolecular proton fraction (MPF) mapping is a recent quantitative MRI method for fast assessment of brain myelination. Information about reproducibility and sensitivity of MPF mapping to magnetic field non-uniformity is important for clinical applications.

Purpose: To assess scan-rescan repeatability and a value of B_0 and B_1 field inhomogeneity corrections in single-point synthetic-reference MPF mapping.

Study Type: Prospective.

Population: 8 healthy adult volunteers underwent two scans with 11.5±2.3 months interval.

Field Strength/Sequence: 3T; whole-brain 3D MPF mapping protocol included three spoiled gradient-echo sequences providing T_1, proton density, and magnetization transfer contrasts with $1.25\times1.25\times1.25$ mm^3 resolution and B_0 and B_1 mapping sequences.

Assessment: MPF maps were reconstructed with B_0 and B_1 field non-uniformity correction, B_0 and B_1 only corrections, and without corrections. Mean MPF values were measured in automatically segmented white matter (WM) and gray matter (GM).

Statistical Tests: Within-subject coefficient of variation (CV), intraclass correlation coefficient (ICC), Bland-Altman plots, and paired t-tests to assess scan-rescan repeatability. Repeated-measures ANOVA to compare field corrections.

Results: Maximal relative local MPF errors without correction in the areas of largest field non-uniformities were about 5% and 27% for B_0 and B_1, respectively. Effect of B_0 correction was insignificant for whole-brain WM ($P>0.25$) and GM ($P>0.98$) MPF. The absence of B_1 correction caused a positive relative bias of 4–5% ($P<0.001$) in both tissues. Scan-rescan agreement was similar for all field correction options with ICCs 0.80–0.81 for WM and 0.89–0.92 for GM. CVs were 1.6–1.7% for WM and 0.7–1.0% for GM.

Corresponding author: Vasily L. Yarnykh, PhD, Department of Radiology, University of Washington, 850 Republican St, Room 255, Seattle, WA 98109, Phone: 1-206-616-0259, Fax: 1-206-616-9354, yarnykh@uw.edu.

Author Manuscript Author Manuscript Author Manuscript Author Manuscript

Data Conclusion: Single-point method enables high repeatability of MPF maps obtained with the same equipment. Correction of B_0 inhomogeneity may be disregarded to shorten the examination time. B_1 non-uniformity correction improves accuracy of MPF measurements at 3T. Reliability of whole-brain MPF measurements in WM and GM is not affected by B_0 and B_1 field corrections.

Keywords

Macromolecular proton fraction; B_0 mapping; B_1 mapping; reproducibility; myelin

INTRODUCTION

Single-point macromolecular proton fraction (MPF) mapping[1,2] is a recently emerged quantitative MRI method based on the magnetization transfer (MT) effect and enabling the assessment of myelination in neural tissues. This method demonstrated strong correlations between MPF and histologically measured myelin density in animal models including the normal rat brain,[3] cuprizone-induced demyelination in mice,[4] and ischemic stroke in rats.[5] In pilot clinical studies, MPF measured by the single-point method showed a promise as a biomarker of myelin in multiple sclerosis (MS),[6,7] mild traumatic brain injury,[8] and during pre-[9–11] and post-natal[11,12] brain development. MPF is defined as the relative amount of macromolecular protons involved into cross-relaxation with water protons and can be mapped by a variety of quantitative MT (qMT) methods.[13–21] Irrespective to the measurement technique, a number of animal studies[3–5,22–24] confirmed sensitivity of MPF or related measures to the myelin content changes validated by histology. The single-point MPF mapping method[1,2] provides an attractive time-efficient approach for clinical translation of MPF measurements. This method relies on the MPF fit within the single-parameter single-point algorithm[1] in isolation from other two-pool model parameters thus enabling a substantial scan time reduction due to the use of the minimal number of source images. In the fastest design based on the synthetic reference image reconstruction,[2] only three spoiled gradient-echo (GRE) images providing MT, T_1, and proton density (PD) contrast weightings are needed to obtain an MPF map. In addition to these basic images, the method is typically executed with specialized sequences for B_0 and B_1 field mapping, which are used in the reconstruction algorithm[1,2] to correct for errors in the offset frequency and flip angles. Recent studies[25,26] have suggested that MPF measured using a traditional multi-parameter two-pool model fit method can be rather insensitive to B_1-related errors under certain conditions.

The use of MPF as a biomarker in clinical studies requires the knowledge of accuracy and precision of the method, as well as understanding of the sources and magnitude of potential instrumental errors. In this context, elimination of unessential correction scans may be beneficial for the method in view of both scan time reduction and exclusion of additional sources of noise. Thus the objectives of this study were to characterize scan-rescan repeatability and a role of B_0 and B_1 field inhomogeneity corrections in the single-point synthetic-reference MPF mapping method.

Author Manuscript Author Manuscript Author Manuscript Author Manuscript

MATERIALS AND METHODS

Simulations

To investigate potential errors in MPF measurements caused by B_0 and B_1 field inhomogeneities, signal intensities of PD-, T_1-, and MT-weighted source images were simulated for a series of field non-uniformity factors and then used to compute MPF by the single-point synthetic reference algorithm[2] with nominal values of field-dependent pulse sequence parameters. Source signal intensities were generated using the matrix two-pool pulsed steady-state model detailed elsewhere.[1] B_0 field errors were modelled by computing MT-weighted signal intensities with the offset frequency shift corresponding to the B_0 non-uniformity factor equal to the difference between actual and nominal B_0 (B_{0a}–B_{0n}). To model B_1 errors, all flip angles in all component sequences were multiplied by the B_1 non-uniformity factor equal to the ratio of the actual to nominal B_1 field strength (B_{1a}/B_{1n}). Simulations were carried out for the two sets of tissue two-pool model parameters representing brain white matter (WM) and gray matter (GM).[1] The following parameters were used: MPF=13%; T_1=1 s; reverse cross-relaxation rate constant R=19.0 s^{-1}; T_2 of free water protons, T_2^F=22 ms; and T_2 of macromolecular protons, T_2^B=10 μs for WM and MPF=6.5%; T_1=1.5 s; R=19.0 s^{-1}; T_2^F=33 ms; and T_2^B=10 μs for GM. T_1 values of the water and macromolecular proton pools were assumed equal to the observed T_1.[1] Pulse sequence parameters were identical to those detailed in the experimental protocol outlined below. Simulations were performed using custom-written C-language software.

Study Population

The study was approved by the Institutional Review Board and all participants provided written informed consent. Data were obtained from eight healthy volunteers (four females and four males). The mean age ± standard deviation (SD) was 44.6 ± 12.2 years (range 29–66 years). Study participants underwent two repeated imaging examinations with the mean interval ± SD of 11.5 ± 2.3 months (range 7–14 months).

MRI Acquisition

Images were acquired on a 3 T whole-body scanner (Achieva; Philips Medical Systems, Best, Netherlands) with an eight-channel head coil. The 3D MPF mapping protocol was implemented according to the single-point synthetic reference method[2] and included the following imaging sequences:

1. MT-weighted GRE: TR = 28 ms, flip angle (FA) = 10°, scan time 5 min 48 s;
2. PD-weighted GRE: TR = 21 ms, FA = 4°, scan time 4 min 21 s; and
3. T_1-weighted GRE: TR = 21 ms, FA = 25°, scan time 4 min 21 s.

Off-resonance saturation in the MT-weighted sequence was achieved by the single-lobe sinc pulse with Gaussian apodization, offset frequency 4 kHz, effective saturation FA = 560°, and duration 12 ms. All images were acquired with dual-echo readout (TE_1/TE_2 = 2.3 ms/6.9 ms), FOV = 240×240×180 mm^3, and actual voxel size of 1.25×1.25×1.25 mm^3 interpolated to 0.63×0.63×0.63 mm^3 after zero-padded reconstruction. Additionally, 3D dual-echo B_0 maps[27] ($TR/TE_1/TE_2$ = 20/2.3/3.3 ms, FA = 10°, voxel size 2.5×2.5×2.5 mm^3, scan time 2

Author Manuscript Author Manuscript Author Manuscript Author Manuscript

min 8 s) and actual flip-angle imaging (AFI) B_1 maps[28] ($TR_1/TR_2/TE$= 40/160/2.3 ms, FA = 60°, voxel size 2.5×2.75×5.0 mm^3, scan time 3 min 26 s) were obtained in the same geometry and interpolated to the 0.63×0.63×0.63 mm^3 voxel size. Parallel imaging (SENSE) was used for all scans in two phase encoding directions with acceleration factors 1.5 and 1.2. In all sequences, non-selective excitation and optimal spoiling[29] with the excitation pulse phase increments of 169° for GRE and 39° for AFI were used.

Image Processing and Analysis

Prior to map reconstruction, individual echo images in each dataset were averaged to increase SNR.[30] Then extracranial tissues were removed from source images by applying a brain mask created from the PD-weighted image using the brain extraction tool[31] available in FSL software (FMRIB Software Library; http://www.fmrib.ox.ac.uk/fsl). MPF maps were reconstructed according to the single-point synthetic reference algorithm[2] using custom-written C-language software with the previously determined[1] constraints for the non-adjustable two-pool model parameters (R=19.0 s^{-1}, ratio T_2^F/T_1=0.022, and T_2^B=10 μs). Four types of reconstruction were carried out: with B_0 and B_1 field non-uniformity correction, with B_0 correction only, with B_1 correction only, and without field corrections. MPF fit was performed after exclusion of voxels containing cerebrospinal fluid (CSF) by applying a threshold of T_1=3 s to T_1 maps, which are computed as an intermediate step in the MPF reconstruction algorithm. MPF maps reconstructed with each technique were segmented into three tissue classes: WM, GM, and a mixed class corresponding to the voxels including partial volume of CSF (PVCSF) to account for incomplete CSF removal. Segmentation was performed using the automated tool FAST[32] in FSL software. MPF maps were segmented in the native image space with the Markov random field weighting parameter 0.25 and process initialization with tissue-specific priors equal to the following MPF values: 12% for WM, 6% for GM, and 1% for PVCSF. Mean values calculated within each tissue mask were used for subsequent analyses.

Statistical Analysis

Normality of MPF values was assessed using the Shapiro-Wilk test for each tissue class. Since no significant departures from the normal distribution were identified, further analyses were carried out using parametric statistics. Scan-rescan repeatability was assessed by the within-subject coefficient of variation (CV) and intraclass correlation coefficient (ICC) for each tissue class and reconstruction type. ICC estimates were obtained using an average-measures absolute-agreement two-way mixed-effects model. One-sample t-tests for the mean differences were used to detect a possible bias between MPF measurements from repeated scans in each tissue with each field correction option. To examine the effect of field corrections across repeated scans, two-way repeated-measures ANOVA model was used with two within-subject factors (scan number with two levels and reconstruction type with four levels) for each tissue class. Greenhouse-Geisser correction for non-sphericity was applied to the degrees of freedom. The biases between reconstruction options were assessed in a series of post-hoc pairwise comparisons between the means of repeated scans with the Tukey honest significant difference (HSD) correction for multiple tests. Bland-Altman plots were used to investigate an agreement between repeated scans and field correction types across brain tissues. The limits of agreement were calculated as the mean difference ±

Author Manuscript Author Manuscript Author Manuscript Author Manuscript

1.96SD of the mean difference. Two-tailed tests were used in all analyses with the significance level of $P<0.05$. Most analyses were carried out in Statistica (StatSoft Inc, Tulsa, OK, USA) software. ICCs and CVs were calculated using SPSS (SPSS Inc, Chicago, IL, USA) software.

RESULTS

Simulations of MPF errors caused by B_0 and B_1 field inhomogeneities

Simulated dependences of MPF measurement errors on B_0 and B_1 field non-uniformity factors are plotted in Fig 1. Deviations of MPF from the true value showed nearly linear behavior in a typically occurring range of B_0 and B_1 non-uniformities at 3T. Simulations predicted larger absolute errors for WM as compared to GM (Fig. 1a,b). However, these errors appeared fairly proportional to the tissue MPF resulting in similar relative errors (Fig 1c,d). Simulations indicated a substantially larger effect of B_1 as compared to B_0. The absolute bias caused by B_1 field inhomogeneity approached about 4% for WM and 2% for GM in the extreme case of the 50% B_1 field drop, which corresponds to the lowest margin of B_1 non-uniformity over the human head at 3 T. For the largest B_0 field shifts (up to 450 Hz), which can be observed in the proximity to air-tissue interfaces around paranasal sinuses, predicted absolute MPF errors were around 1% for WM and 0.5% for GM. In the relative scale, the maximal local MPF errors caused by B_0 and B_1 inhomogeneity in the human brain were estimated as 7.5% and 35%, respectively.

Effect of B_0 and B_1 corrections on MPF maps

Example MPF, B_0 and B_1 maps, segmentation masks, and effects of different field correction options are illustrated in Fig. 2. While original MPF maps (Fig. 2a) did not show visible distinctions related to field non-uniformity corrections due to sharp tissue contrast (images for different reconstructions are not shown), the MPF difference maps (Fig 2e–h) highlighted field-dependent MPF variations. The difference maps calculated by subtracting the uncorrected map from either fully corrected (B_0 and B_1) (Fig. 1e) or B_1 only corrected (Fig. 2g) maps demonstrated apparent propagation of B_1 non-uniformities into MPF measurements. In the areas of B_1 field drop, an increase in uncorrected MPF translated into negative voxel values in the difference maps. MPF errors caused by B_1 inhomogeneity appeared tissue-dependent and approached about 3.5% in the absolute scale (≈27% in the relative scale) for WM in the regions with the lowest B_1 field ($B_{1a}/B_{1n}\approx0.6$), as seen in Fig. 2e,g. In contrast, B_0 non-uniformity correction produced a minor effect with an about 0.6% maximal absolute MPF difference (≈5% relative error) for the largest B_0 shift, $B_{0a}–B_{0n}\approx410$ Hz, observed in WM of the gyrus rectus (Fig. 2f). Impact of B_0 correction was very small regardless of the presence of B_1 correction (Fig. 2f,h). These findings appeared in close agreement with simulation results described above (Fig. 1).

Statistics of MPF measurements in brain tissues across different field correction options and repeated scans is summarized in Table 1. Pairwise comparisons between field corrections are presented in Table 2 and illustrated by Bland-Altman plots in Fig. 3. Repeated-measures ANOVA revealed the highly significant effect of field correction on MPF values in all tissues ($F(1.15, 8.04)=873.8$, $P<0.001$ for WM; $F(1.10, 7.68)=488.9$, $P<0.001$ for GM; and $F(1.01,$

Author Manuscript Author Manuscript Author Manuscript Author Manuscript

7.05)=34.5, P <0.001 for PVCSF) and no significant effect of repeated scans (F(1, 7)=0.8, P=0.41 for WM; F(1, 7)=2.2, P=0.18 for GM; and F(1, 7)=0.3, P=0.59 for PVCSF). Significant negative differences of similar magnitude were found between either fully corrected or B_1 only corrected and uncorrected MPF maps in all tissues (Table 2, Fig. 3a,c). Additionally, fully corrected and B_1 corrected MPF maps showed similar quantitative distinctions from B_0 corrected MPF maps (Table 2). All the above biases were nearly identical in the absolute values within each tissue and corresponded to about 4–5% relative MPF measurement errors. At the same time, no significant differences were identified between B_0 corrected and uncorrected MPF maps, as well as between fully corrected and B_1 corrected MPF maps (Table 2). Bland-Altman plots (Fig. 3b,d) demonstrated that MPF measurements within these pairs were virtually identical. Collectively, the above observations indicate that B_1 correction significantly reduces a field-related bias in MPF measurements, while the effect of B_0 correction is negligible. If B_0 and B_1 corrections are combined, their overall effect on the whole-brain MPF measurements can be attributed to B_1 correction alone.

Scan-rescan repeatability of MPF measurements

Bland-Altman plots characterizing scan-rescan repeatability of MPF measurements with each field correction option are presented in Fig. 4. No significant bias between repeated MPF measurements was identified (Table 1). For all field corrections, nearly equivalent scan-rescan agreement was observed (Table 1, Fig. 4). In the tissues of practical interest (WM and GM), scan-rescan variability was low with CVs of 1.6–1.7% for WM and 0.7–1.0% for GM (Table 2). ICCs for repeated measurements in each brain tissue were in a range of 0.8–0.9, which indicates good overall reliability, especially in view of relatively small between-subject variability. MPF in WM showed higher within-subject variability than MPF in GM (Table 1, Fig. 4).

DISCUSSION

The knowledge about reproducibility and inherent instrumental errors is of paramount importance for applications of any quantitative imaging method in clinical studies. The fast single-point MPF mapping method offers a clinically targeted approach for quantitative monitoring of myelin content changes in both WM and GM in various neurological conditions and in the course of brain development.[6–12] The present study evaluated scan-rescan repeatability and potential errors related to the absence of B_0 and B_1 field non-uniformity corrections in single-point synthetic-reference MPF mapping at 3T in a single-center setting. The findings of this study demonstrate that the method provides excellent repeatability with no significant errors caused by B_0 inhomogeneity and a relatively small bias associated with B_1.

Non-uniform distribution of B_0 and B_1 magnetic fields is a critical factor affecting accuracy of many quantitative MRI techniques. Historically, correction of B_0 and B_1 inhomogeneities has been widely used in qMT protocols based on both single- and multi-point off-resonance saturation methods.[1,2,6–8,13,33] The results of this study indicate that the magnitude of B_0-related errors in single-point MPF mapping is very small and practically negligible for the

Author Manuscript Author Manuscript Author Manuscript Author Manuscript

global measurements in brain tissues. Accordingly, the method can be safely used without B_0 correction, particularly, if whole-brain WM and GM metrics are of interest. Elimination of a B_0 mapping sequence enables an about 2 minute examination time reduction for the whole-brain 3D protocol. However, care must be taken in the applications targeted to the brain areas proximal to the paranasal sinuses and mastoid bone, which are vulnerable to severe B_0 field distortions. If accurate local MPF measurements in such regions are of interest, acquisition of a B_0 map still may be beneficial.

In contrast to B_0, this study demonstrates that B_1 correction in fast MPF mapping generally cannot be eliminated without the risk of systematic errors. However, such errors appeared relatively small for global brain tissue measurements, thus suggesting that in certain situations acquisition of B_1 maps may also be discarded. One is related to longitudinal studies performed in a single-center setting and focused on within-subject effects with whole-brain MPF measures as outcomes. In such studies, a minor constant bias usually is not a concern, while geometrical patterns of B_1 field non-uniformity are not expected to change over time for the same subject and excitation coil. Our results justify this approach, because B_1 field inhomogeneity correction does not affect measurement reliability as evidenced by similar within-subject CVs and ICCs for corrected and uncorrected MPF maps. Another is the application of fast MPF mapping at 1.5 T or lower magnetic field strengths. The feasibility of such applications has been recently demonstrated.[9–12] B_1 inhomogeneity at 1.5 T is about four-fold smaller than that at 3 T[34] with typical variations of the non-uniformity factor across the brain in a range of 0.9–1.05.[28,35] Approximation of the results of this study to 1.5 T imaging suggests that B_1-related errors in WM and GM MPF measurements are expected to be negligible with the global bias around 1% and maximal local errors <7% in the relative scale.

The physical origin of B_0- and B_1-related errors in fast MPF mapping can be understood based on the simplified pulsed model of the two-pool magnetization exchange.[14] To conceptualize the main effects determining the sensitivity of MPF measurements to B_0 and B_1 field inhomogeneities, it is convenient to transform the expression for MT ratio (MTR) derived earlier[14] and given by Eq. 21 with coefficients defined by Eqs. 24 and 25 therein.[14] Neglecting a contribution from a relatively small excitation FA in the MT-weighted sequence, applying the relation between the forward (k) and reverse (R) rate constants, $R=k(1\text{-MPF})/\text{MPF}$, and assuming that $R_1=1/T_1 \ll R$, the equation for MTR can be approximated as

$$\text{MTR} \approx \frac{R T_1 \text{MPF} \left\langle W^B \right\rangle}{R + \left\langle W^B \right\rangle + R T_1 \text{MPF} \left\langle W^B \right\rangle} \quad (1)$$

where $\left\langle W^B \right\rangle = \pi T_{MT} TR^{-1} \left\langle \omega_1^2 \right\rangle g^B\left(\triangle, T_2^B \right)$ is the time-averaged saturation rate for macromolecular protons[1,14] defined through the parameters of the saturation pulse (root-mean-square amplitude $\langle \omega_1^2 \rangle$ and duration T_{MT}) and a function of the offset frequency Δ, $g^B(\Delta, T_2^B)$, given by the SuperLoentzian spectral lineshape.[13,14] MTR is convenient to use in this context as a measure of an extent of signal saturation in the MT-weighted image. The effect of B_0 can be explained by a change in the saturation rate W^B due to the offset

Author Manuscript Author Manuscript Author Manuscript Author Manuscript

frequency shift. Particularly, a local increase of B_0 field results in a high-frequency shift of water and macromolecular resonances, which effectively reduces the offset frequency of the off-resonance saturation pulse specified relative to the whole-sample water signal. This leads to an unaccounted increase of the saturation effect (MTR in Eq. 1), which translates into an overestimated MPF when nominal Δ is used in the single-point algorithm.[1,2] The small magnitude of B_0-related errors is due to a smooth dependence of g^B on Δ.[1,14] The effect of B_1 field non-uniformity is more complex and can be decomposed into the two main factors: the error in the saturation power applied in the MT-weighted sequence and the error in the T_1 estimate derived from the variable FA (VFA) images and supplied into the single-point algorithm.[1,2] These effects drive MPF estimation in opposite directions. Specifically, a decrease of B_1 field reduces the saturation rate W^B proportionally to $<\omega_1^2>$ and results in a reduced MTR (Eq, 1), which translates into underestimation of MPF computed at nominal ω_1. On the other hand, a decrease of actual flip angles applied during VFA data acquisition results in T_1 underestimation proportional to the squared B_1 field non-uniformity factor.[36] If W^B and MTR in Eq. 1 are assumed constant, a reduced T_1 will be compensated by MPF overestimation. Both effects are rather strong, as they have quadratic dependence on the B_1 non-uniformity factor. However, their partial cancellation explains the fact that B_1-related errors in MPF are much smaller than those in T_1. For example, a 50% reduction of B_1 field would result in about four-fold underestimation of T_1[36] and only 35% overestimation of MPF as detailed above. Generalization of this mechanism of B_1-related error formation to multi-point qMT techniques also provides a simple explanation of the recently published[25] somewhat paradoxal observation that T_1 measured by the VFA method enables more immune to B_1 non-uniformity MPF measurements than T_1 measured by the B_1-insensitive inversion-recovery technique. This finding is caused by the fact that the errors in the saturation rate remain uncompensated after elimination of B_1-related errors from T_1.

As compared to multi-point multi-parameter qMT techniques, the single-point method appears more sensitive to B_1 field non-uniformities. It was recently demonstrated that a multi-point qMT acquisition scheme[25] provides MPF error range from +7 to −3% for the B_1 non-uniformity factor range of 0.7–1.3, and it can be further reduced by the optimal design of the acquisition protocol.[26] Our results suggest that for the same B_1 non-uniformity range, errors in MPF measured by the single-point method are in a range ±18–20%. It should be pointed out that in multi-point techniques,[25,26] reduced B_1 sensitivity can be achieved by combining data points obtained with low and high FA of the saturation pulse, whereas this approach is inapplicable to the single point method.[1,2] From the practical standpoint, single-point MPF mapping in combination with any fast B_1 mapping sequence provides a much more time-efficient approach to measure MPF than multi-point techniques. It also enables whole-brain high-resolution volumetric MPF mapping, which is virtually impossible with multi-point acquisition. Furthermore, a relatively small range of B_1-related errors allows relaxed requirements on the accuracy and quality of B_1 measurements used for correction of MPF maps, thus offering flexibility in the choice of a B_1 mapping technique.

This study demonstrates excellent repeatability of MPF measurements by the single-point method with remarkably low within-subject CVs. Similarly high repeatability with CVs in a range of 1–2% was reported for this technique applied to the mouse brain in vivo.[4] As compared to other quantitative brain imaging methods including T_1 and T_2 relaxometry,

Author Manuscript Author Manuscript Author Manuscript Author Manuscript

diffusion tensor imaging, and MTR mapping, CVs for scan-rescan agreement in single-point MPF mapping appeared on the lowest end of the values reported in the literature.[37–39] Notably, the single-point method substantially reduces variability of repeated MPF measurements relative to the multi-point technique,[33] which showed an average CV of 4.7%.[33] It is important to emphasize that our results were obtained with a rather long interval between scans (about 1 year), which is typical for longitudinal treatment or progression studies in chronic diseases, such as MS.[40] Accordingly, the estimates of inherent MPF mapping variability reported in this study can be directly applied to planning future clinical trials with MPF values in automatically segmented brain tissues as outcome measures.

This study has several limitations. First, repeatability of MPF mapping was evaluated in a single-platform single-center setting. More research is needed to assess reproducibility of the method across MRI platforms of different manufacturers and units of the same manufacturer. Second, MPF measurements were focused on global brain tissue metrics, which showed a promise as clinical biomarkers in brain diseases.[6–8] Additional studies may be needed for MPF measurements in specific anatomic structures in conjunction with appropriate segmentation procedures. Third, this study employed an optimized research pulse sequence and protocol.[1,2] Recent implementations of the fast MPF mapping protocol with unmodified manufacturers' sequences in clinical settings[9–12] may provide different sensitivity to B_0 and B_1 field inhomogeneity, which needs to be evaluated separately. Fourth, this study involved healthy population, while repeatability in patients with a specific disease may need to be assessed for more rigorous design of clinical trials.

In conclusion, this study provides a methodological foundation for applications of the single-point synthetic-reference MPF mapping method in longitudinal clinical brain studies. Fast MPF mapping enables high repeatability of MPF measurements in segmented brain tissues, being one of the most reliable quantitative brain MRI techniques. Correction of B_0 field inhomogeneity can be safely disregarded in the majority of MPF mapping applications to shorten the examination time. B_1 non-uniformity correction is recommended to obtain accurate MPF measurements using the single-point method in 3 T magnetic field. Reliability of whole-brain MPF measurements in WM and GM is not affected by the application of B_0 and B_1 inhomogeneity correction, either separately or concurrently.

ACKNOWLEDGEMENTS

The authors thank Ms. Svetlana Kildyaeva for manuscript proofreading.

Grant support:

Recruitment and data acquisition, Contract grant sponsor: National Multiple Sclerosis Society; Contract grant number: RG 4864A1/1. Image processing and analysis, Contract grant sponsor: Ministry of Education and Science of the Russian Federation within the State Assignment Project; Contract grant number: 18.2583.2017/4.6. Simulation software, Contract grant sponsor: National Institutes of Health (NIH); Contract grant number: R24NS104098-01A1. Numerical simulations and manuscript preparation, Contract grant sponsor: Russian Science Foundation; Contract grant number: 19-75-20142.

REFERENCES

1. Yarnykh VL. Fast macromolecular proton fraction mapping from a single off-resonance magnetization transfer measurement. Magn Reson Med 2012;68:166–178. [PubMed: 22190042]

Author Manuscript Author Manuscript Author Manuscript Author Manuscript

2. Yarnykh VL. Time-efficient, high-resolution, whole brain three-dimensional macromolecular proton fraction mapping. Magn Reson Med 2016;75:2100–2106. [PubMed: 26102097]
3. Underhill HR, Rostomily RC, Mikheev AM, Yuan C, Yarnykh VL. Fast bound pool fraction imaging of the in vivo rat brain: Association with myelin content and validation in the C6 glioma model. Neuroimage 2011;54:2052–2016. [PubMed: 21029782]
4. Khodanovich MY, Sorokina IV, Glazacheva VY, et al. Histological validation of fast macromolecular proton fraction mapping as a quantitative myelin imaging method in the cuprizone demyelination model. Sci Rep 2017;7:46686. [PubMed: 28436460]
5. Khodanovich MY, Kisel AA, Akulov AE, et al. Quantitative assessment of demyelination in ischemic stroke in vivo using macromolecular proton fraction mapping. J Cereb Blood Flow Metab 2018;38:919–931. [PubMed: 29372644]
6. Yarnykh VL, Bowen JD, Samsonov A, et al. Fast whole-brain three-dimensional macromolecular proton fraction mapping in multiple sclerosis. Radiology 2015;274:210–220. [PubMed: 25208343]
7. Yarnykh VL, Krutenkova EP, Aitmagambetova G, et al. Iron-insensitive quantitative assessment of subcortical gray matter demyelination in multiple sclerosis using the macromolecular proton fraction. AJNR Am J Neuroradiol 2018;39:618–625. [PubMed: 29439122]
8. Petrie EC, Cross DJ, Yarnykh VL, et al. Neuroimaging, Behavioral, and Psychological Sequelae of Repetitive Combined Blast/Impact Mild Traumatic Brain Injury in Iraq and Afghanistan War Veterans. J Neurotrauma 2014;31:425–436. [PubMed: 24102309]
9. Yarnykh VL, Prihod'ko IY, Savelov AA, Korostyshevskaya AM. Quantitative assessment of normal fetal brain myelination using fast macromolecular proton fraction mapping. AJNR Am J Neuroradiol 2018;39:1341–1348. [PubMed: 29748201]
10. Korostyshevskaya AM, Prihod'ko IY, Savelov AA, Yarnykh VL. Direct comparison between apparent diffusion coefficient and macromolecular proton fraction as quantitative biomarkers of the human fetal brain maturation. J Magn Reson Imaging 2019;50:52–61. [PubMed: 30635965]
11. Korostyshevskaya AM, Savelov AA, Papusha LI, Druy AE, Yarnykh VL. Congenital medulloblastoma: Fetal and postnatal longitudinal observation with quantitative MRI. Clin Imaging 2018;52:172–176. [PubMed: 30096555]
12. Yarnykh V, Knipenberg N, Tereshchenkova O. Quantitative assessment of pediatric brain myelination in a clinical setting using macromolecular proton fraction. In: Proceedings of the 26th Annual Meeting of ISMRM, Paris, France; 2018 (abstract 525).
13. Sled JG, Pike GB. Quantitative imaging of magnetization transfer exchange and relaxation properties in vivo using MRI. Magn Reson Med 2001;46:923–931. [PubMed: 11675644]
14. Yarnykh VL. Pulsed Z-spectroscopic imaging of cross-relaxation parameters in tissues for human MRI: theory and clinical applications. Magn Reson Med 2002;47:929–939. [PubMed: 11979572]
15. Ramani A, Dalton C, Miller DH, Tofts PS, Barker GJ. Precise estimate of fundamental in-vivo MT parameters in human brain in clinically feasible times. Magn Reson Imaging 2002;20:721–731. [PubMed: 12591568]
16. Ropele S, Seifert T, Enzinger C, Fazekas F. Method for quantitative imaging of the macromolecular 1H fraction in tissues. Magn Reson Med 2003;49:864–871. [PubMed: 12704769]
17. Yarnykh VL, Yuan C. Cross-relaxation imaging reveals detailed anatomy of white matter fiber tracts in the human brain. NeuroImage 2004;23:409–424. [PubMed: 15325389]
18. Gochberg DF, Gore JC. Quantitative magnetization transfer imaging via selective inversion recovery with short repetition times. Magn Reson Med 2007;57:437–441. [PubMed: 17260381]
19. Gloor M, Scheffler K, Bieri O. Quantitative magnetization transfer imaging using balanced SSFP. Magn Reson Med 2008;60:691–700. [PubMed: 18727085]
20. Soellinger M, Langkammer C, Seifert-Held T, Fazekas F, Ropele S. Fast bound pool fraction mapping using stimulated echoes. Magn Reson Med 2011;66:717–724. [PubMed: 21437973]
21. van Gelderen P, Jiang X, Duyn JH. Rapid measurement of brain macromolecular proton fraction with transient saturation transfer MRI. Magn Reson Med 2017;77:2174–2185. [PubMed: 27342121]
22. Odrobina EE, Lam TY, Pun T, Midha R, Stanisz GJ. MR properties of excised neural tissue following experimentally induced demyelination. NMR Biomed 2005;18:277–284. [PubMed: 15948233]

Author Manuscript Author Manuscript Author Manuscript Author Manuscript

23. Janve VA, Zu Z, Yao SY, et al. The radial diffusivity and magnetization transfer pool size ratio are sensitive markers for demyelination in a rat model of type III multiple sclerosis (MS) lesions. Neuroimage 2013;74:298–305. [PubMed: 23481461]
24. Thiessen JD, Zhang Y, Zhang H, et al. Quantitative MRI and ultrastructural examination of the cuprizone mouse model of demyelination. NMR Biomed 2013;26:1562–1581. [PubMed: 23943390]
25. Boudreau M, Stikov N, Pike GB. B(1) -sensitivity analysis of quantitative magnetization transfer imaging. Magn Reson Med 2018;79:276–285. [PubMed: 28349596]
26. Boudreau M, Pike GB. Sensitivity regularization of the Cramér-Rao lower bound to minimize B(1) nonuniformity effects in quantitative magnetization transfer imaging. Magn Reson Med 2018;80:2560–2572. [PubMed: 29733460]
27. Skinner TE, Glover GH. An extended two-point Dixon algorithm for calculating separate water, fat, and B0 images. Magn Reson Med 1997;37:628–630. [PubMed: 9094088]
28. Yarnykh VL. Actual flip-angle imaging in the pulsed steady state: a method for rapid three-dimensional mapping of the transmitted radiofrequency field. Magn Reson Med 2007;57:192–200. [PubMed: 17191242]
29. Yarnykh VL. Optimal radiofrequency and gradient spoiling for improved accuracy of T1 and B1 measurements using fast steady-state techniques. Magn Reson Med 2010;63:1610–1626. [PubMed: 20512865]
30. Helms G, Dechent P. Increased SNR and reduced distortions by averaging multiple gradient echo signals in 3D FLASH imaging of the human brain at 3T. J Magn Reson Imaging 2009;29:198–204. [PubMed: 19097114]
31. Smith SM. Fast robust automated brain extraction. Hum Brain Mapp 2002;17:143–155. [PubMed: 12391568]
32. Zhang Y, Brady M, Smith S. Segmentation of brain MR images through a hidden Markov random field model and the expectation-maximization algorithm. IEEE Trans Med Imaging 2001;20:45–57. [PubMed: 11293691]
33. Levesque IR, Sled JG, Narayanan S, et al. Reproducibility of quantitative magnetization-transfer imaging parameters from repeated measurements. Magn Reson Med 2010;64:391–400. [PubMed: 20665783]
34. Liu W, Collins CM, Delp PJ, Smith MB. Effects of end-ring/shield configuration on homogeneity and signal-to-noise ratio in a birdcage-type coil loaded with a human head. Magn Reson Med 2004;51:217–221. [PubMed: 14705065]
35. Sled JG, Pike GB. Standing-wave and RF penetration artifacts caused by elliptic geometry: an electrodynamic analysis of MRI. IEEE Trans Med Imaging 1998;17:653–662. [PubMed: 9845320]
36. Helms G, Dathe H, Dechent P. Quantitative FLASH MRI at 3T using a rational approximation of the Ernst equation. Magn Reson Med 2008;59:667–672. [PubMed: 18306368]
37. Gloor M, Scheffler K, Bieri O. Intrascanner and interscanner variability of magnetization transfer-sensitized balanced steady-state free precession imaging. Magn Reson Med 2011;65:1112–1117. [PubMed: 21413076]
38. Jansen JF, Kooi ME, Kessels AG, Nicolay K, Backes WH. Reproducibility of quantitative cerebral T2 relaxometry, diffusion tensor imaging, and 1H magnetic resonance spectroscopy at 3.0 Tesla. Invest Radiol 2007;42:327–337. [PubMed: 17507802]
39. Schwartz DL, Tagge I, Powers K, et al. Multisite reliability and repeatability of an advanced brain MRI protocol. J Magn Reson Imaging 2019;50:878–888. [PubMed: 30652391]
40. Bakshi R, Minagar A, Jaisani Z, Wolinsky JS. Imaging of multiple sclerosis: role in neurotherapeutics. NeuroRx 2005;2:277–303. [PubMed: 15897951]

Author Manuscript
Author Manuscript
Author Manuscript
Author Manuscript

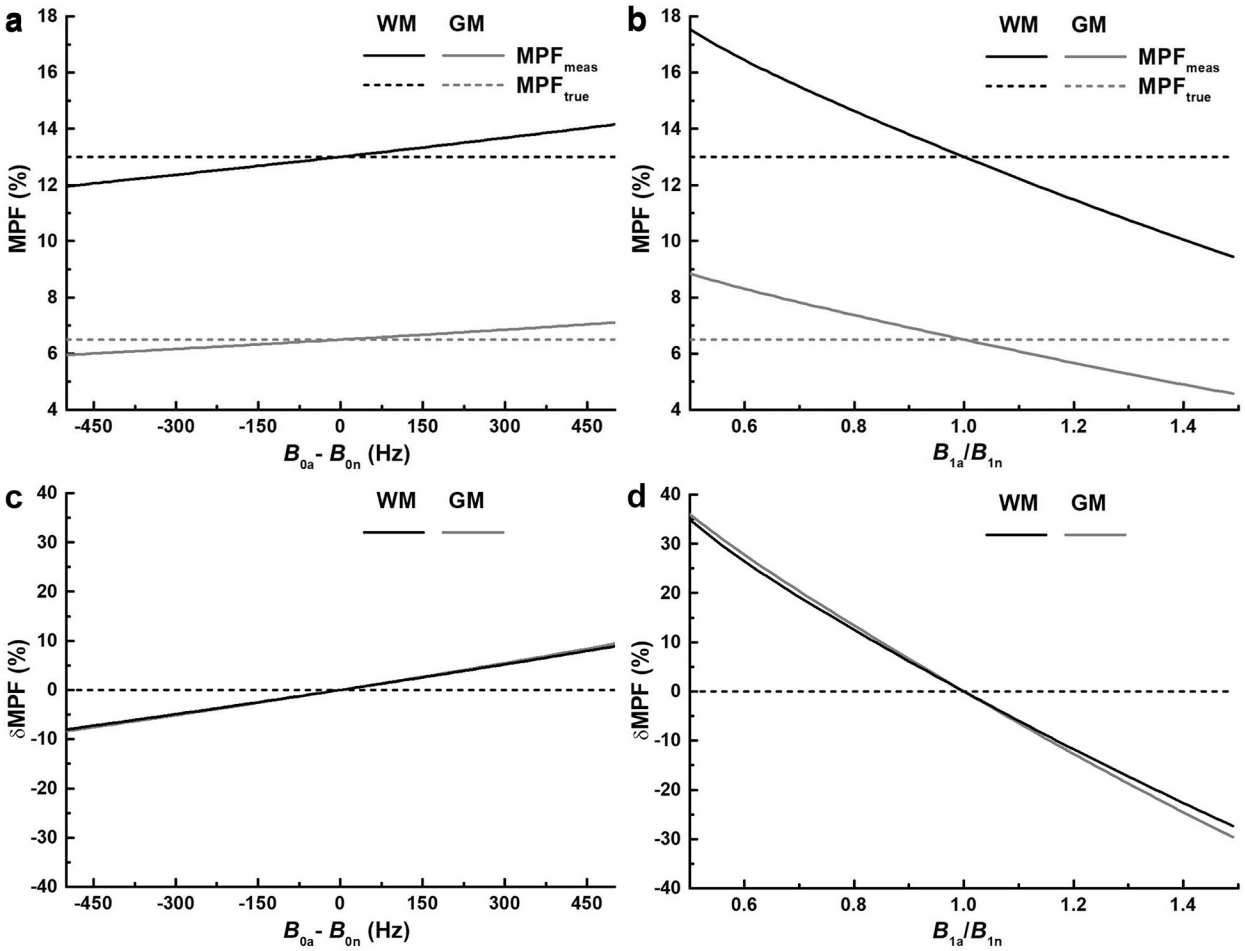

Figure 1.

Simulations of absolute (**a**, **b**) and relative (**c**, **d**) MPF errors caused by non-uniformity of B_0 (**a**, **c**) and B_1 (**b**, **d**) magnetic fields for the parameter sets corresponding to WM (black lines) and GM (gray lines). Dashed horizontal lines in plots (**a**, **b**) indicate true MPF values.

Author Manuscript Author Manuscript Author Manuscript Author Manuscript

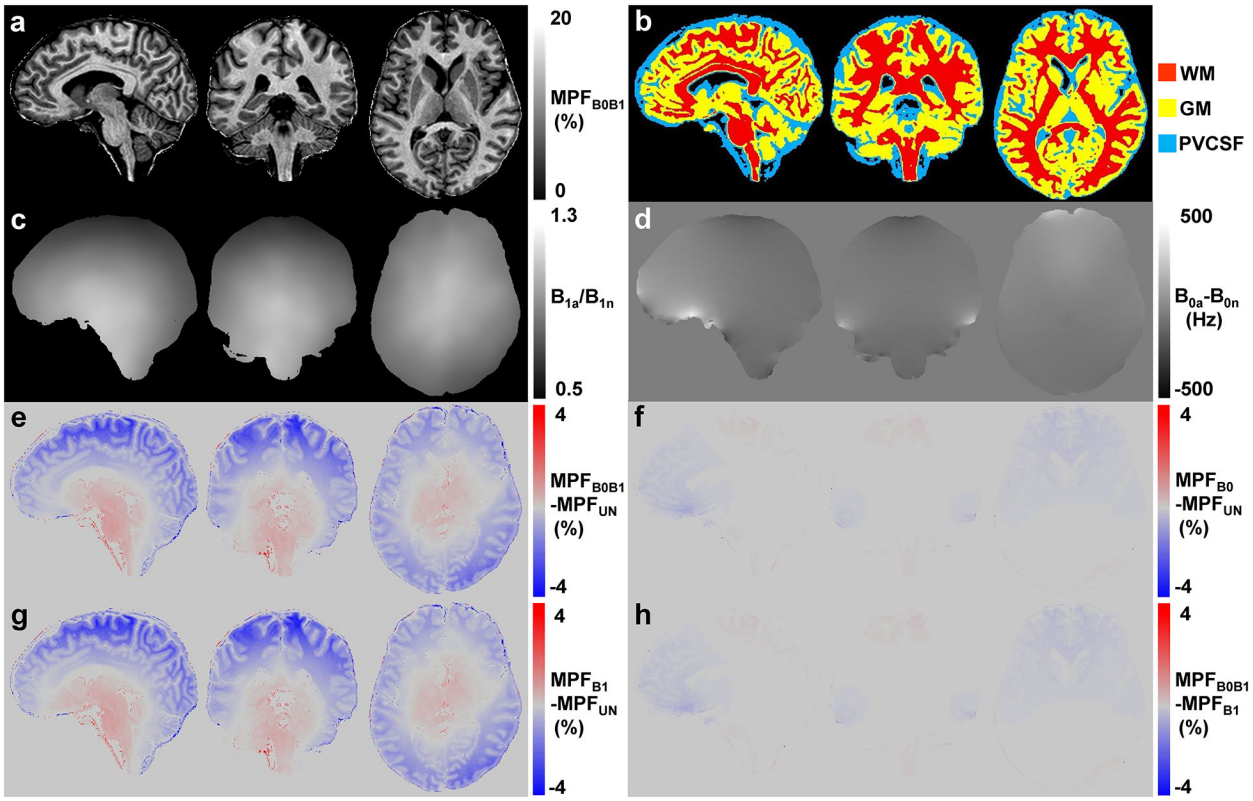

Figure 2.

Effects of B_0 and B_1 field inhomogeneity correction in MPF mapping of the brain: 3D MPF map obtained with B_0 and B_1 field corrections (**a**); segmented tissue masks used for MPF measurements (WM, GM, PVCSF) (**b**); B_1 map (**c**); B_0 map (**d**); difference between MPF maps reconstructed with full correction (B_0 and B_1) and without correction (**e**); difference between MPF maps reconstructed with B_0 correction and without correction (**f**); difference between MPF maps reconstructed with B_1 correction and without correction (**g**); difference between MPF maps reconstructed with full correction and with B_1 correction (**h**). Grayscale ranges correspond to the MPF range 0–20% (**a**), B_1 non-uniformity factor range 0.5–1.3 (**c**), and B_0 non-uniformity factor range −500-+500 Hz (**d**). MPF difference maps are presented in the color scale corresponding to the −4-+4% range (**e**-**h**). Comparison between difference maps (**e**-**h**) demonstrates apparent propagation of B_1 non-uniformities into MPF maps and a negligible effect of B_0 inhomogeneity.

Author Manuscript Author Manuscript Author Manuscript Author Manuscript

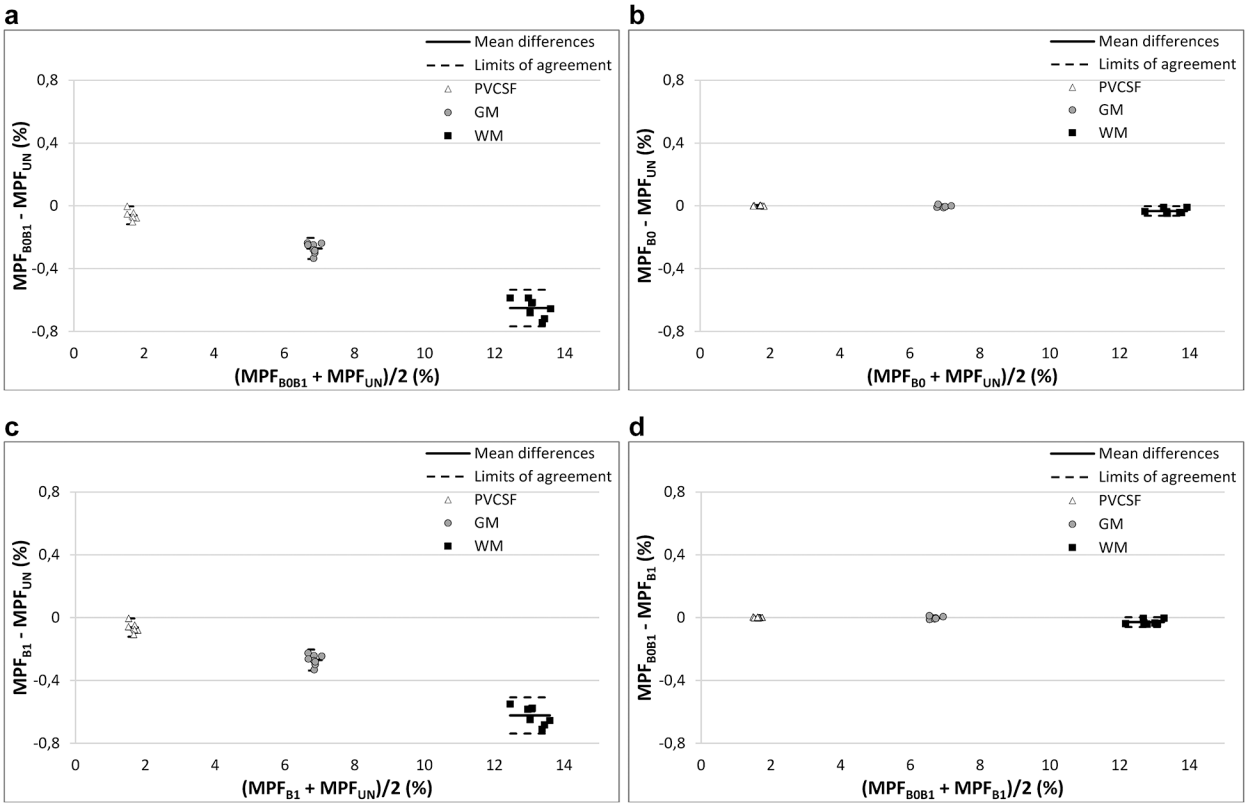

Figure 3.

Bland-Altman plots comparing MPF values in segmented brain tissues (WM, GM, PVCSF) between different field non-uniformity corrections: full correction (B_0 and B_1) vs. no correction (**a**); B_0 correction vs. no correction (**b**); B_1 correction vs. no correction (**c**); and full correction vs. B_1 correction (**d**). Individual data are the means of MPF measurements from two repeated scans. Solid and dashed lines indicate mean differences and limits of agreement, respectively.

Author Manuscript Author Manuscript Author Manuscript Author Manuscript

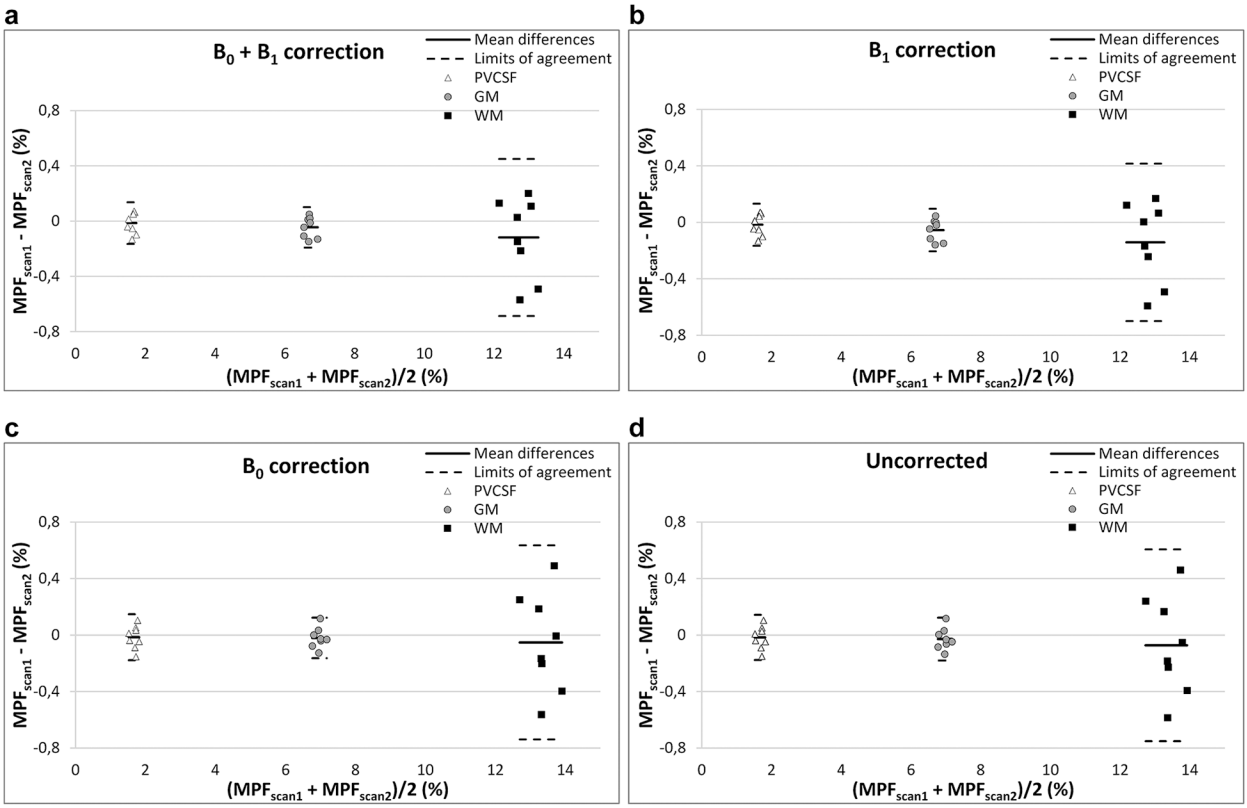

Figure 4.

Bland-Altman plots for scan-rescan repeatability of MPF measurements in segmented brain tissues (WM, GM, PVCSF) obtained with different field non-uniformity corrections: full correction (B_0 and B_1) (**a**); B_1 correction (**b**); B_0 correction (**c**); and no correction (**d**). Solid and dashed lines indicate mean differences and limits of agreement, respectively.

Author Manuscript Author Manuscript Author Manuscript Author Manuscript

Table 1.

Repeatability statistics for MPF measurements in brain tissues with different field non-uniformity corrections.

	B_0 + B_1 corrected	B_0 corrected	B_1 corrected	Uncorrected
WM				
MPF for scan 1 (%)	12.73±0.32	13.38±0.38	12.74±0.32	13.40±0.38
MPF for scan 2 (%)	12.85±0.40	13.43±0.45	12.89±0.40	13.47±0.45
Mean MPF of scans (%)	12.79±0.33	13.41±0.38	12.82±0.33	13.44±0.37
Mean MPF difference of scans (%)	−0.12±0.29	−0.05±0.35	−0.14±0.28	−0.07±0.35
P for mean difference[a]	0.29	0.69	0.20	0.57
CV (%)	1.62	1.74	1.65	1.74
ICC	0.81	0.80	0.80	0.80
GM				
MPF for scan 1 (%)	6.67±0.12	6.95±0.14	6.67±0.12	6.95±0.14
MPF for scan 2 (%)	6.71±0.13	6.97±0.13	6.72±0.14	6.98±0.13
Mean MPF of scans (%)	6.69±0.12	6.96±0.13	6.69±0.12	6.96±0.13
Mean MPF difference of scans (%)	−0.05±0.07	−0.02±0.07	−0.05±0.08	−0.03±0.08
P for mean difference[a]	0.13	0.47	0.08	0.36
CV (%)	0.88	0.72	0.95	0.78
ICC	0.89	0.92	0.87	0.91
PVCSF				
MPF for scan 1 (%)	1.62±0.10	1.68±0.11	1.62±0.10	1.62±0.10
MPF for scan 2 (%)	1.63±0.09	1.70±0.11	1.63±0.09	1.63±0.09
Mean MPF of scans (%)	1.63±0.09	1.69±0.10	1.63±0.09	1.63±0.09
Mean MPF difference of scans (%)	−0.01±0.08	−0.01±0.08	−0.02±0.08	−0.01±0.08
P for mean difference[a]	0.62	0.63	0.55	0.62
CV (%)	3.15	3.23	3.14	3.15
ICC	0.81	0.85	0.82	0.86

[a] *P* values are from one-sample t-test.

Author Manuscript

Author Manuscript

Author Manuscript

Author Manuscript

Table 2.

Pairwise comparisons between mean MPF measurements in brain tissues obtained with different field non-uniformity corrections.

Correction type pair	Tissue MPF (%): Mean difference ± SD (*P*)[a]		
	WM	GM	PVCSF
B_1+B_0 − Uncorrected	−0.65±0.06 (<0.001)	−0.27±0.03 (<0.001)	−0.06±0.03 (<0.001)
B_0 − Uncorrected	−0.03±0.02 (0.25)	−0.00±0.01 (0.98)	0.00±0.00 (1.00)
B_1 − Uncorrected	−0.62±0.06 (<0.001)	−0.27±0.03 (<0.001)	−0.06±0.03 (<0.001)
B_1+B_0 − B_0	−0.62±0.06 (<0.001)	−0.27±0.03 (<0.001)	−0.06±0.03 (<0.001)
B_1+B_0 − B_1	−0.03±0.02 (0.39)	−0.00±0.01 (1.00)	0.00±0.00 (0.99)
B_1 − B_0	−0.60±0.06 (<0.001)	−0.27±0.03 (<0.001)	−0.06±0.03 (<0.001)

[a] *P* values are from two-way repeated-measures ANOVA with Tukey HSD post-hoc correction.